https://doi.org/10.3311/PPee.24041

Periodica Polytechnica Electrical Engineering and Computer Science

Drone Shaped Fractal Antenna with Defected Ground Structure for RF Energy Harvesting Applications

Mohammed Muataz Hasan[1*], Ahmed M. A. Sabaawi[1]

[1] Electronics Engineering Department, College of Electronics Engineering, Ninevah University, Al-Jawsaq, 41001 Mosul, Ninevah, Iraq
[*] Corresponding author, e-mail: mohammed.muataz.eng22@stu.uoninevah.edu.iq

Received: 11 December 2023, Accepted: 13 May 2024, Published online: 18 June 2024

Abstract

A proposed multiband drone shaped fractal antenna (Antenna-1) is introduced in this paper that targets the most required frequencies used for radio frequency energy harvesting applications, including WLAN-2.4G, WLAN-5G, WLAN-6G, Mobile DCS1700, Mobile LTE and WIMAX services. A novel fractal shape is designed and combined with a standard square geometrical shape in order to implement the front patch of the antenna. The antenna is simulated with CST Studio Suite software and fabricated on FR-4 substrate. Different antenna stages with parametric study and optimization were implemented to get the best performance from the drone shape fractal antenna. The multiband (Antenna-1) supports six resonate frequencies (1.7155 GHz, 2.424 GHz, 3.36 GHz, 3.789 GHz, 5.843 GHz, 6.886 GHz) with peak gain of (2.83 dBi) at the frequency 2.45 GHz and a maximum bandwidth of (0.4281 GHz) at the frequency 5.8 GHz that make it a suitable antenna for radio frequency energy harvesting applications.

Keywords

radio frequency energy harvesting, multiband antenna, fractal shape, defected ground structure (DGS)

1 Introduction

The most conspicuous energy sources used by ambient energy harvesting systems are the wind, solar, thermal, and radio frequencies. The maximum power density collected from the wind source is 177 μW/cm^2, and the maximum power density collected from the radio frequency source is 40 μW/cm^2 [1]. Were each energy harvesting system has its own advantages and disadvantages. The availability of the ambient sources that exist in a specific geographical area on the earth is so important for each type of energy harvesting system. The dominant advantage of the RF ambient source over the other ambient sources is its availability, for example, the radio towers are designed to always be turned on and available to use as transceivers for mobile communications, including GSM/UMTS/WIMAX/LTE/5G services, as well as the wireless routers that exist at each home, office and building and are used as transceivers for communicating with multiple different devices through WLAN-2.4G, WLAN-5G and WLAN-6G services. RF energy is an excellent ambient energy source since it is used for a wide variety of applications, including AM/FM radio, cellular networks, Wi-Fi signals, and digital/analog TV. Also, the electromagnetic radio waves can penetrate through the building's walls and enclosed areas, so they can be used for indoor and outdoor applications. Also, the small size and lightweight of RF energy harvesting systems compared to other types of energy harvesting systems such as (wind turbines) or (solar cell arrays) make it a perfect system for portable applications. This paper is focused on the receiving antenna, which is the most important component of the RF energy harvesting systems since the receiving antenna determines the amount of RF energy that can be collected by the RF energy harvesting system, which is converted to a useful DC voltage by special rectification circuits. The antenna radiation performance (directivity and gain) and the number the resonant frequencies that are supported by the receiving antenna are important for RF energy harvesting systems. The ideal receiving antenna for an RF energy harvesting system should have omnidirectional radiation characteristics with a high gain and should resonate with high number of frequency bands that are supported by different wireless services, including WLAN and cellular networks [1]. The researchers have designed and implemented different types of receiving antennas used by RF energy

Cite this article as: Hasan, M. M., Sabaawi, A. M. A. "Drone Shaped Fractal Antenna with Defected Ground Structure for RF Energy Harvesting Applications", Periodica Polytechnica Electrical Engineering and Computer Science, 2024. https://doi.org/10.3311/PPee.24041

harvesting systems, including low profile antennas and multiband antennas [2–16]. From an RF energy harvesting perspective, multiband antennas can be more useful because they receiving the RF power simultaneously from different radio frequency bands transmitted by different RF sources from different locations [17]. Fractal antennas are considered multiband antennas because they can generate multiband and wideband frequency response on a single antenna [18, 19]. In this paper, a multiband fractal antenna with a drone shape geometry has been designed and simulated with CST Studio Suite software [20], then implemented on an FR-4 substrate due to its low profile and low cost. Also, a new fractal shape has been designed and used to implement the modified square patch, which is the cornerstone structure of this proposed antenna. The antenna supports multiple frequency bands that are used by different wireless services, including wireless local area networks and cellular networks that are required for RF energy harvesting applications.

2 Fractal shape design

The design of the new fractal shape starts with an initiator line with a length of (L) as shown in Fig. 1(a), The first iteration translates the initiator line to (8) eight equal lines with a length of (L/8) for each of them to form the shape shown in Fig. 1(b) The next steps are to expand the shape of the first iteration by two operations the first one is to mirror it on the (Y) axis as shown in Fig. 1(c). Then mirror it on the (X) axis to form the shape shown in Fig. 1(d). The final shape is shown in Fig. 1(e).

3 Antenna construction

Multiband antennas can be constructed from combining fractal shapes with one of different geometrical shapes [19] like triangles, square, pentagonal, hexagonal, etc. as shown in Fig. 2(c). The first stage of the proposed drone shaped antenna is implemented firstly by modifying the standard square patch sides in Fig. 2(a) with the fractal shape that was designed previously in Fig. 1(e). This will create the modified square patch shown in Fig. 2(b) and this patch will be the cornerstone for implementing the drone shaped antenna.

The total length (Lt) for each side of the modified square patch can be calculated with Eq. (1):

$$Lt = \left(\frac{x}{4}\right)+\left(\frac{x}{8}\right)+\left(\frac{x}{8}\right)+\left(\frac{x}{4}\right)+\left(\frac{x}{4}\right)+\left(\frac{x}{4}\right) + \left(\frac{x}{8}\right)+\left(\frac{x}{8}\right)+\left(\frac{x}{4}\right)+\left(\frac{x}{8}\right)+\left(\frac{x}{8}\right) = 2x \quad (1)$$

The perimeter of the modified square patch = $4 \times 2x = 8x$.

The perimeter of the standards square patch = $4x$.

The perimeter ratio between the modified square patch and the standard square patch = $8x / 4x = 2x$.

It's clear from the previous calculations that the electrical length for each side of the standard square patch will be doubled by a factor of 2 after the modifications. This is the main advantage of the fractal antenna, which creates longer electrical lengths and increasing the perimeter length of the geometrical shape and also generates more frequencies by using different electrical lengths that correspond to the wavelength (λ) for each operating frequency [18].

All the antennas in this paper have been simulated with CST Studio Suite software. A standard FR-4 substrate with dielectric constant $\varepsilon r = 4.3$, a thickness of 1.6 mm and a loss tangent (δ) of 0.025 was utilized, Perfect Electrical Conductor (PEC) material selected for creating the front patch and the

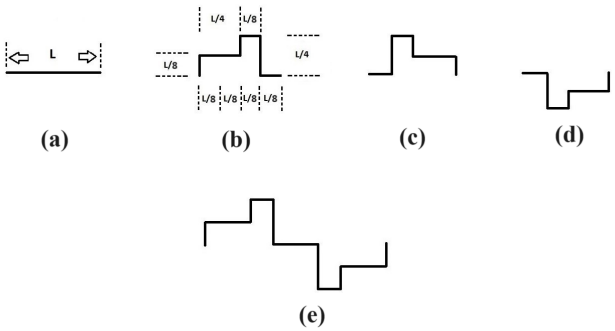

Fig. 1 Fractal Shape Design; (a) The Initiator line; (b) The first iteration; (c) Mirror shape (b) on Y axis; (d) Mirror shape (c) on X axis; (e) The final shape design

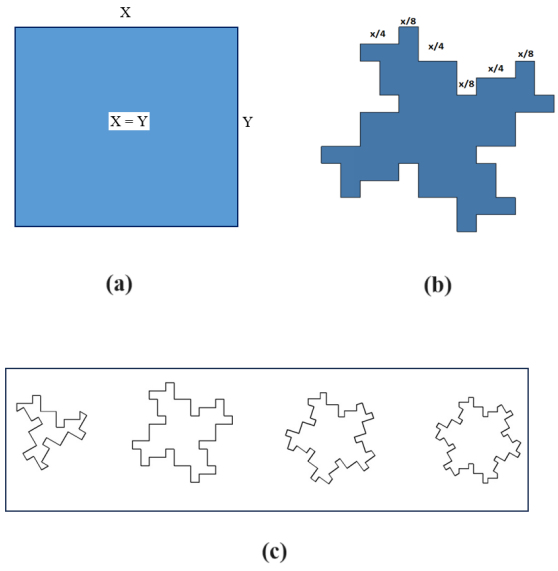

Fig. 2 Antenna Construction; (a) Standard square patch; (b) Modified square patch; (c) Modified Geometrical Shapes

back ground plane with [0.035 mm] of thickness. The first stage of the proposed antenna is constructed from the modified square patch that is shown in Fig. 2(b), whereas the second stage is implemented by copying and scaling down the modified square patch of the first stage using scale factor of S = 0.5, then put four of the scaled down modified square patches at each corner of the modified patch at stage 1. The third stage implemented by copied and scaling down the modified square patch of the first stage using scale factor of S = 0.25, then put three of them at each corner of the modified square patches that was created on the second stage. This will create the final antenna design as shown in Fig. 3.

The dimensions for each stage of the proposed antenna are shown in Fig. 3.

A Full ground substrate and feeding inset width of [1 mm] were implemented in the beginning of designing the drone shaped antenna. Later at the advanced design stage, a defected ground structure (DGS) with slot cut in the front patch was implemented in order to get the optimal results.

4 Impact of number of stage on Antenna-1

For multiband antenna, the reflection coefficient S_{11} is the main antenna parameter that shows the antenna

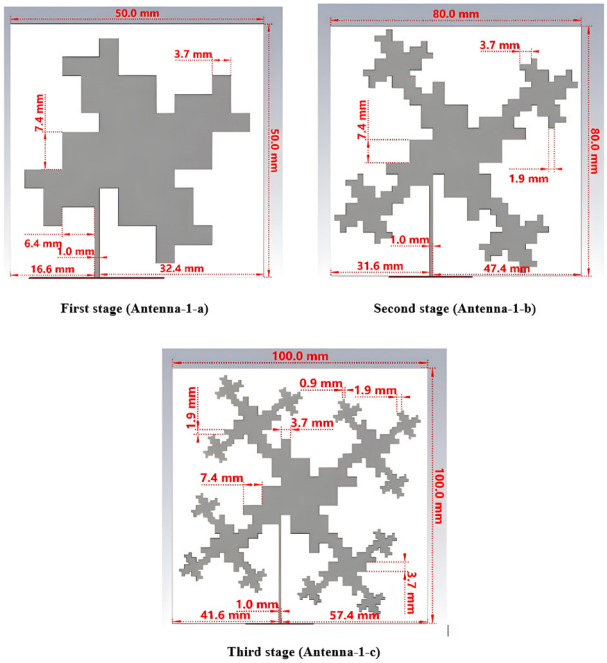

Fig. 3 The dimensions for each stage of the drone shaped antenna

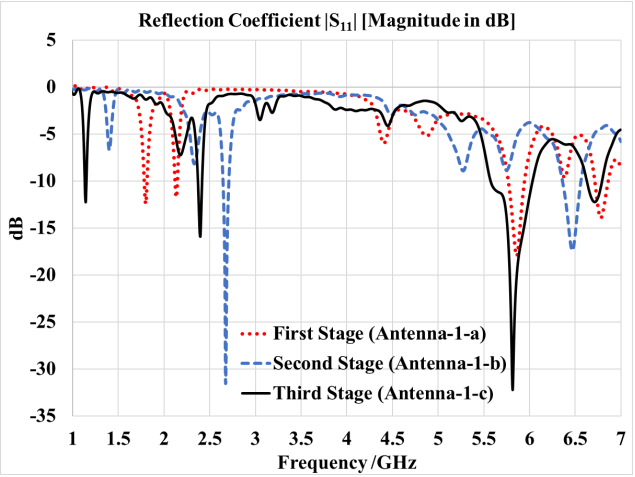

Fig. 4 Simulated results of the Reflection coefficient S_{11} for each stage of the drone shaped antenna

characteristics and performance at each frequency. Fig. 4 shows the simulated results of the reflection coefficient S_{11} for each implemented stage of Antenna-1. The simulated results of the reflection coefficient S_{11} showed that the first stage (Antenna-1-a) resonating at four frequencies (6.7 GHz) and (5.86 GHz) and (2.1 GHz) and (1.8 GHz) and for the second stage (Antenna-1-b) resonating at two frequencies (6.4 GHz) and (2.6 GHz) and for the third stage (Antenna-1-c) resonating at four frequencies (6.7 GHz) and (5.8 GHz) and (2.4 GHz) and (1.1 GHz). The third stage has been selected and studied since it showed the best results that meet the needs for RF energy harvesting applications since it supports the frequencies of interest WLAN 2.4 GHz and WLAN 5 GHz. As shown in Table 1.

5 Parametric analysis for the proposed selected (Antenna-1-c)

As mentioned previously (Antenna-1-c) will be carefully studied in this paper.

5.1 Impact of scale up on (Antenna 1-c)

The scaling process on the (Antenna-1-c) has a major impact on its performance, since the dimension of the patch antenna will be changed and resulting to change the electrical length of the radiator (Front Metal Patch) that corresponds to the wavelengths of the signal (λ) that inversely proportional to the operating frequency and will result to shift the resonating frequencies left or right of the frequency spectrum that

Table 1 Simulated results of Reflection coefficient S_{11} Magnitude in [dB] for each stage of the drone shaped antenna

Antenna Stage	Resonating Frequencies	Simulated results of Reflection coefficient S_{11} [dB]
First Stage (Antenna-1-a)	(6.7 GHz), (5.86 GHz), (2.1 GHz), (1.8 GHz)	(−13.95 dB), (−17.99 dB), (−11.74 dB), (−12.44 dB)
Second Stage (Antenna-1-b)	(6.4 GHz), (2.6 GHz)	(−17.44 dB), (−31.34 dB)
Third Stage (Antenna-1-c)	(6.7 GHz), (5.8 GHz), (2.4 GHz), (1.1 GHz)	(−12.22 dB), (−32.23 dB), (−15.92 dB), (−12.21 dB)

depend on scale up or scale down the antenna. Fig. 5 shows the effect of scaling up (Antenna-1-c) on the reflection coefficient S_{11} for different scale up factors (1.2), (1.5), (1.7). It's clear from Fig. 5 that when increase the scale of the (Antenna-1-c), all the frequencies will be shifted to the left of the frequency spectrum and the value of the reflection coefficient S_{11} for each frequency will be increased i.e. diminished. this will result the lower frequencies be vanished.

5.2 Impact of scale down on (Antenna 1-c)

Fig. 6 shows the reflection coefficient S_{11} simulated results for different scale down factors (0.8), (0.6), (0.3) applied to (Antenna-1-c). It's clear from Fig. 6 that when decrease the scale of the (Antenna-1-c) all the frequencies will be shifted to the right of the frequency spectrum. Also the simulated results show the frequencies (2.4 GHz) and (1.1 GHz) shifted to the right of the frequency spectrum and the frequency (6.7 GHz) and (5.8 GHz) vanished since the frequency spectrum range studied are from (1 GHz to 7 GHz). Also, the value of the reflection coefficient S_{11} decreased i.e. improved for the scale factor = (0.8) and (0.5) for the frequencies (2.4 GHz) and (1.1 GHz). The simulated results confirmed that the resonating frequencies are dependent on the electrical lengths of the (Antenna-1-c) radiator patch that directly impacts the wavelength (λ) for each operating frequency.

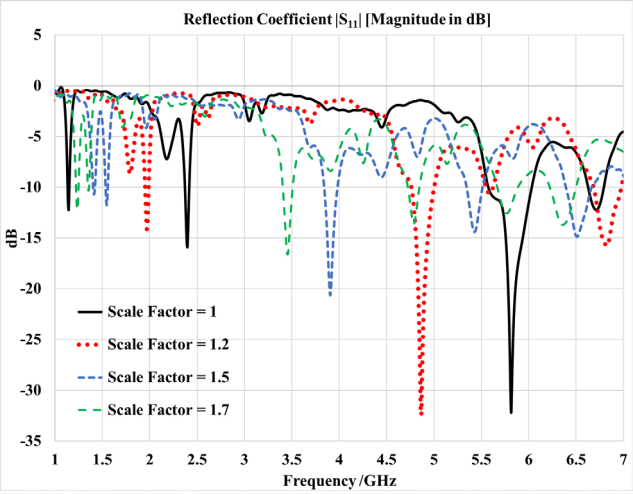

Fig. 5 Simulated results of Reflection coefficient S_{11} for different scale up factor of (Antenna-1-c)

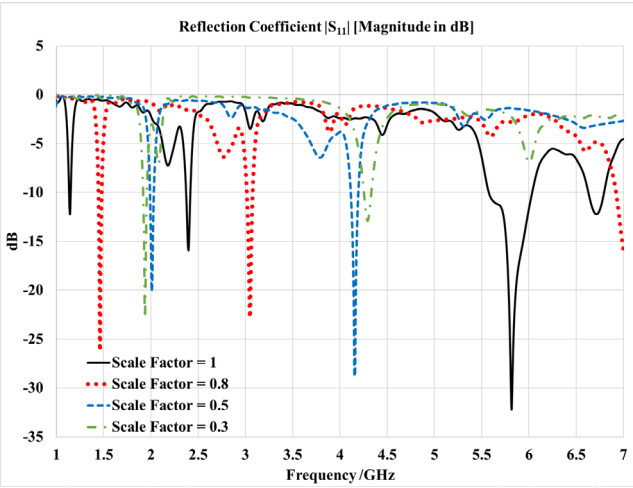

Fig. 6 Simulated results of Reflection coefficient S_{11} for different scale down factor of (Antenna-1-c)

5.3 Impact of changing the ground plane length for (Antenna 1-c)

A lot of research was made to study the effects of changing the dimensions or shape of the ground plane of the Microstrip patch antenna. It's confirmed that there is an impact on the performance of the antenna bandwidth, radiation pattern, gain, and shifting the resonating frequency [21]. Fig. 7 shows the simulated results for the reflection coefficient S_{11} after changing the ground plane length for (Antenna 1-c) for the values [25 mm, 50 mm, 75 mm, 100 mm] and keeping the ground plane width constant for [100 mm]. The best and optimal simulated results from Fig. 7 is by keeping the ground plane length for (Antenna 1-c) to be 100 mm.

5.4 Impact of changing the ground plane width for (Antenna 1-c)

Fig. 8 shows the simulated results for the reflection coefficient S_{11} after changing the ground plane width for (Antenna 1-c) for the values [25 mm, 50 mm, 75 mm, 100 mm] with keeping the ground plane length constant for [100 mm], The simulated results showed major impact on the reflection coefficient S_{11} when changing the ground

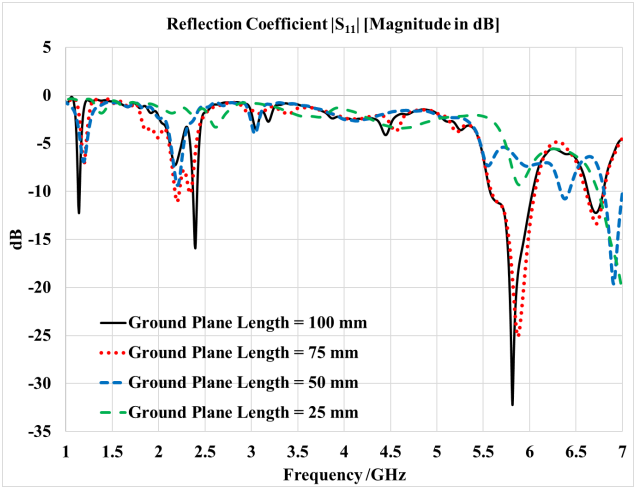

Fig. 7 Simulated results of Reflection coefficient S_{11} for different ground plane length of (Antenna-1-c)

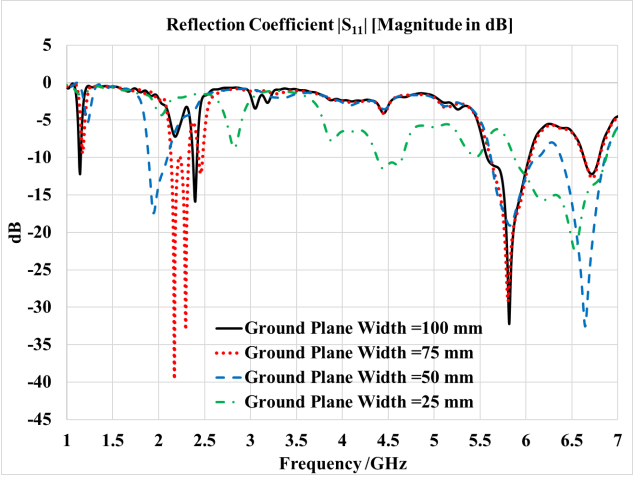

Fig. 8 Simulated results of Reflection coefficient S_{11} for different ground plane width of (Antenna-1-c)

plane width from [100 mm] to [75 mm], this will generate new frequency band from (2.13 GHz to 2.32) with reflection coefficient S_{11} magnitude of [−39.6 dB], and the reflection coefficient S_{11} magnitude increased for the frequency bands (5.8 GHz) and (2.4 GHz) and (1.1 GHz), Also for the simulated results showed the impact of changing the ground width from [100 mm] to [50 mm] will shift the frequency band (2.4 GHz) to the left and shift frequency band (5.8 GHz) to the right of the frequency spectrum.

5.5 Impact of changing feeding inset width for (Antenna 1-c)

Different feeding inset width values [1 mm, 2 mm, 3 mm, 4 mm] for (Antenna-1-c) were applied and Simulated, Fig. 9 shows the simulated results for the reflection coefficient S_{11}. The simulated results shows that increasing the feeding inset width for (Antenna-1-c) will increase

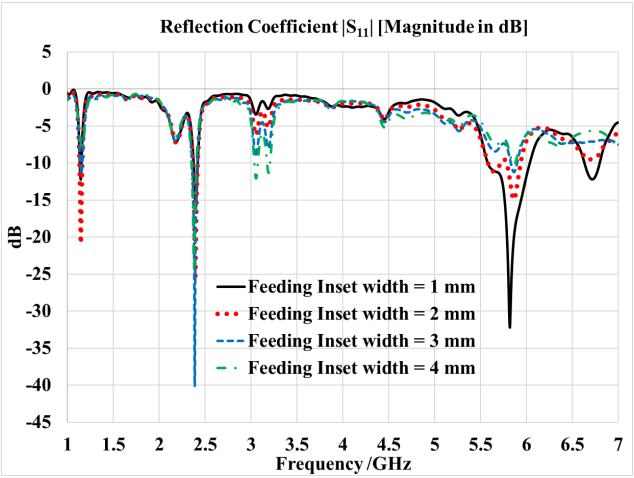

Fig. 9 Simulated results of Reflection coefficient S_{11} for different feeding inset width of (Antenna-1-c)

the magnitude of the reflection coefficient S_{11} for some frequencies while decrease it for others without any frequency shifting also the frequency band (6.7 GHz) has been disappeared, This is the major impact for increasing the feeding inset width since it's directly affect the matching impedance of the Antenna.

6 (Antenna-1-c) Optimization

To get the optimum results from (Antenna-1-c), new modifications were introduced, (slot cut) were applied to the front patch the (Radiator) of (Antenna-1-c) also defected ground structure (DGS) were applied to antenna ground plane [21]. Firstly, the slots were implemented by scaling down the modified square patches that were previously created on different antenna stages shown on Fig. 3 with scale factor of S = 0.25, Then subtract it from the center of all modified square patches for each stage to implement the new optimized (Antenna-1-d) that shown in Fig. 10. Also, the new defected ground structure is implemented by scale up the front patch with scale factor of S = 1.1 then subtract the front patch (Radiator) from the full square ground plane on the back of the substrate to create the new defected ground structure that shown in Fig. 10 Also, the feeding inset shifted by [0.82 mm] to the left as shown in the dimensions of the optimized (Antenna 1-d) in Fig. 11.

7 Comparison between optimized (Antenna-1-d) and (Antenna-1-c)

The simulated results of the reflection coefficient S_{11} for the optimized (Antenna-1-d) shows major performance improvements compared to the results of (Antenna-1-c) as shown in Fig. 12, More resonating frequencies appeared in the frequency spectrum (3.789 GHz, 3.36 GHz, 1.7155 GHz), Also the bandwidth increased significantly For the resonating frequencies (2.4 GHz) and (5.7 GHz), Table 2 shows more details for the optimized (Antenna-1-d) bandwidth, Gain and Directivity in [dBi] also the

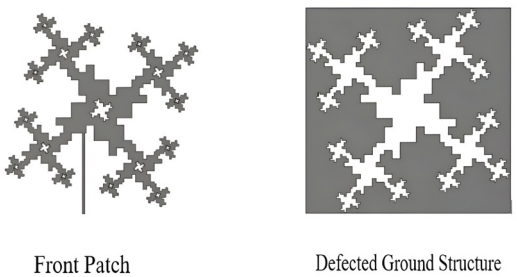

Fig. 10 Front patch with slot cut and the defected ground structure of (Antenna-1-d)

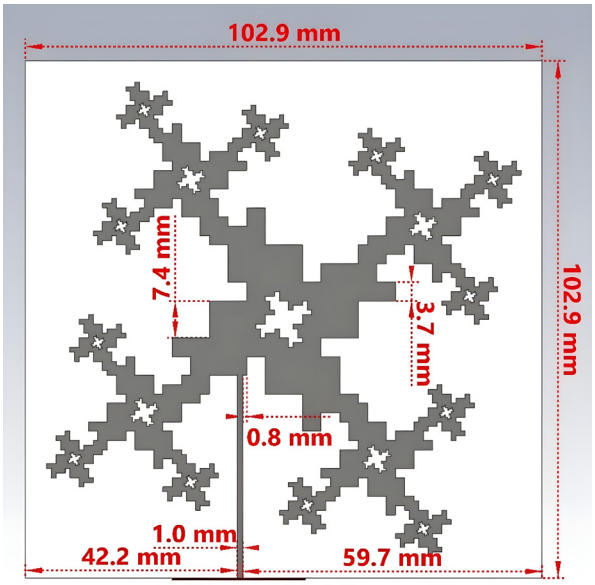

Fig. 11 The Dimensions for the optimized (Antenna-1-d)

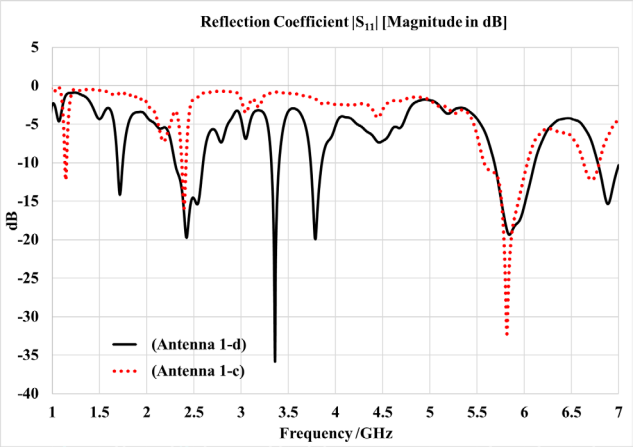

Fig. 12 Simulated results of the Reflection coefficient S_{11} for the optimized (Antenna-1-d) and (Antenna-1-c)

wireless RF applications for each resonating frequency supported by optimized (Antenna-1-d).

Fig. 13 shows the simulated 3D radiation pattern of the directivity magnitude in [dBi] for some of (Antenna-1-d) supported frequencies. Also, Fig. 14 shows the simulated 2D radiation pattern.

8 Discussion and experimental results

The optimized drone shaped fractal antenna is fabricated using PCB technology on FR-4 substrate as shown in Fig. 15. Furthermore, Fig. 16 shows a comparison result of the normalized 2D radiation pattern between the simulated and the practical (Antenna-1-d). Also, Fig. 17 shows comparison results of the reflection coefficient S_{11} magnitude in [dB] between the simulated and the practical fabricated (Antenna-1-d). Fig. 18 shows the experimental setup and the testing environment. In addition, the results show that the proposed antenna has performance improvements compared to other proposed works shown in Table 3. Since the proposed optimized antenna supports more resonating frequencies, that covers more wireless services needed for RFEH applications. Also, the proposed antenna (Antenna 1-d) achieved a good gain for most of its operating frequencies with respect to its size and thickness, given that it has a much smaller substrate area than [4, 13], and [14] , and is much thinner than [4, 7, 11], and [14]. It should be mentioned as well that the FR-4 substrate is less expensive than the (Rogers RT6002), (Arlon 25N), and (Rogers 3003) substrates, and the gain of any antenna is directly proportional to its physical size and thickness [22].

Table 2 Simulated results for the final design of the proposed drone shaped antenna (Antenna-1-d) after optimization

Resonating Frequency (GHz)	Return Loss (S_{11}) (dB)	Minimum Frequency (GHz)	Maximum Frequency (GHz)	Band width (GHz)	Directivity (dBi)	Peak Gain (dBi)	Applications
1.7155	−14.15	1.6901	1.7463	0.056216	4.603	2.785 dBi @ 1.7458 GHz	Mobile DCS 1700, Mobile LTE
2.424	−19.73	2.299	2.5978	0.29883	5.196	2.83 dBi @ 2.45 GHz	WLAN, WIMAX, Mobile LTE
3.36	−35.83	3.3206	3.4036	0.083023	5.504	−0.79 dBi @ 3.36 GHz	WIMAX, Mobile LTE
3.789	−19.9	3.7373	3.8561	0.11883	4.017	−1 dBi @ 3.856 GHz	WIMAX, Mobile LTE
5.843	−19.36	5.6835	6.1116	0.4281	6.404	2.51 dBi @ 5.8512 GHz	WLAN, WIMAX, Mobile LTE
6.886	−15.33	6.7797	7.007	0.2273	6.895	2.165 dBi @ 6.886 GHz	WLAN, Mobile LTE

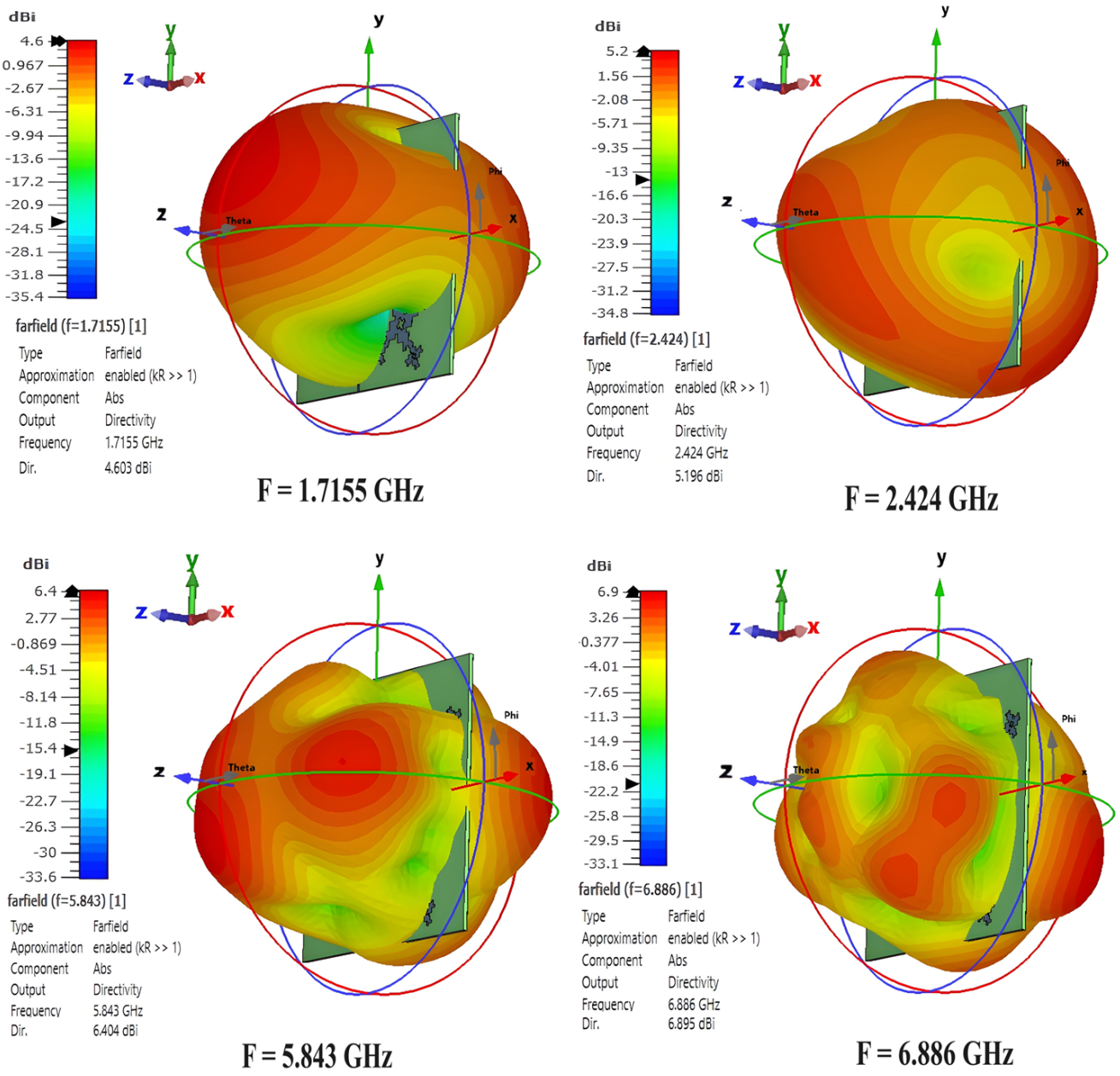

Fig. 13 Simulated 3D radiation pattern of the Directivity magnitude in [dBi] for some of (Antenna-1-d) supported frequencies

9 Conclusion

The proposed multiband fractal drone shaped antenna was carefully studied and modified step by step to achieve some of the requirements of RF energy harvesting applications. The optimized antenna (i.e. Antenna-1-d) targets the RF frequencies of WLAN 2.4G, WLAN 5G, WLAN 6G, WIMAX, Mobile DCS1700, and Mobile LTE services, three stages of (Antenna-1) were designed and simulated which are (Antenna-1-a), (Antenna-1-b), (Antenna-1-c) using CST Studio Suite software and only the optimized version the (Antenna-1-d) was fabricated using FR-4 substrate. Different techniques including defected ground structure (DGS) and slot cuts were implemented during the optimization process to reach the final design of the proposed Antenna-1 (i.e. Antenna-1-d), The simulated results showed that (Antenna-1-d) has a good directivity and gain for most of the supported frequencies also the measurement results of the reflection coefficient S_{11} and the normalized 2D radiation pattern showed acceptable tolerance error with the simulated results taking into account the fabrication difficulties due to the fine detail of fractal geometries that implemented on both of the front patch and back defected ground structure of the antenna also the small slot cuts, and the imperfect testing

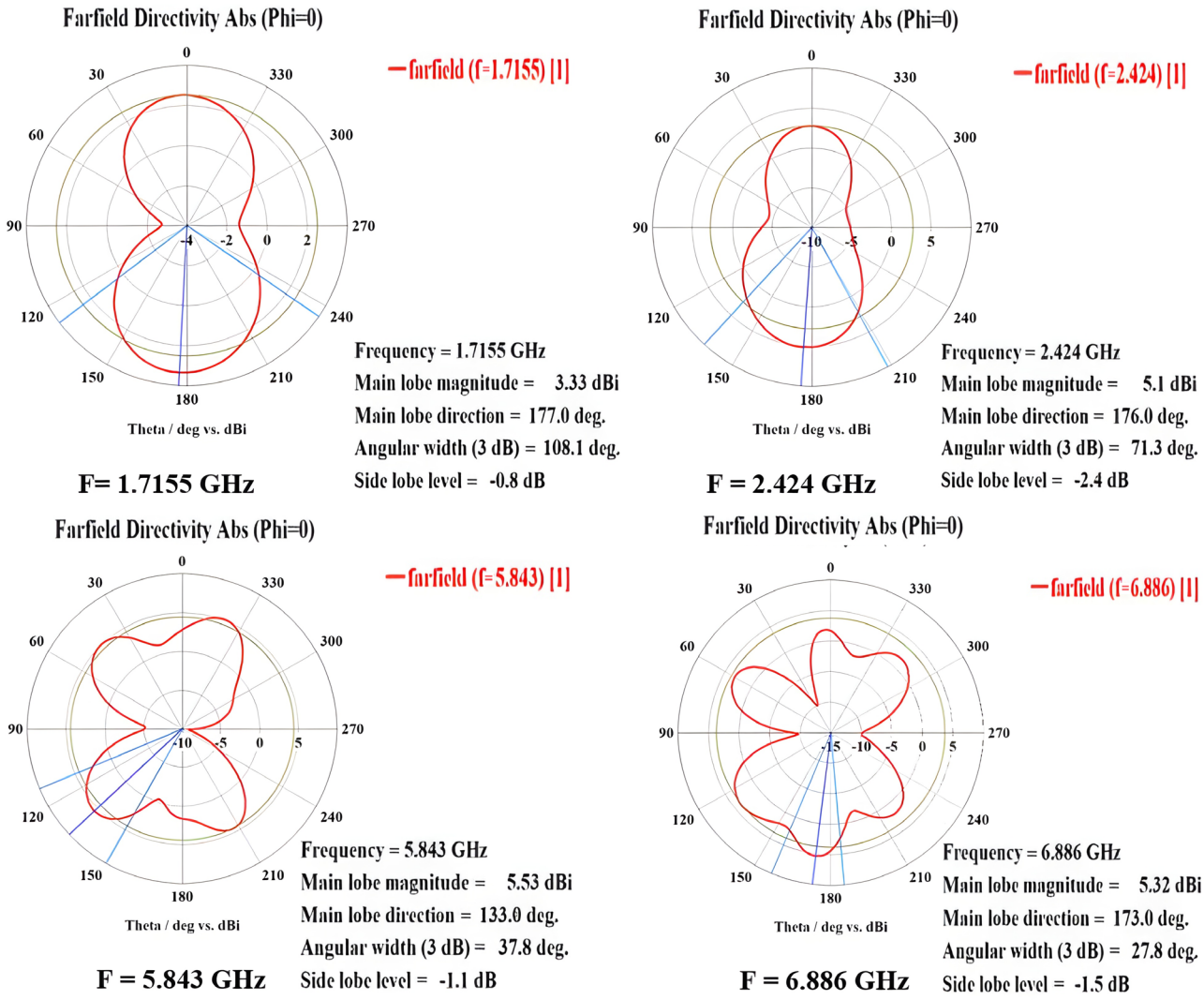

Fig. 14 Simulated 2D radiation pattern of the Directivity magnitude in [dBi] for some of (Antenna-1-d) supported frequencies

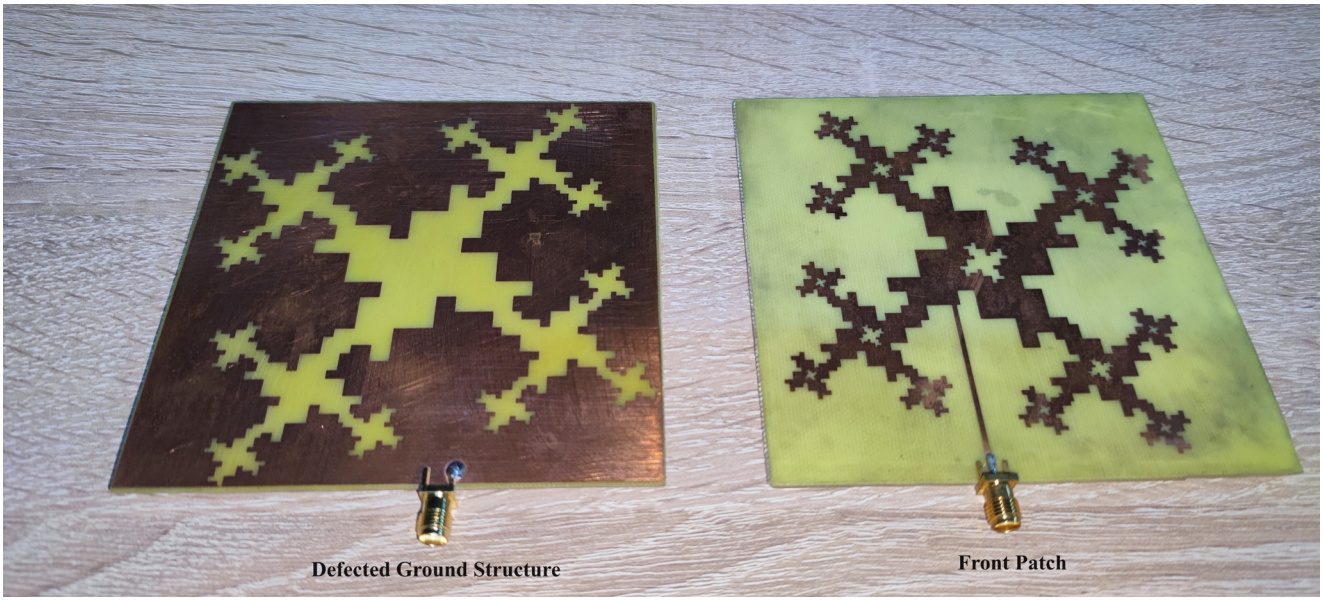

Fig. 15 Photograph of the physical structure of the proposed (Antenna-1-d)

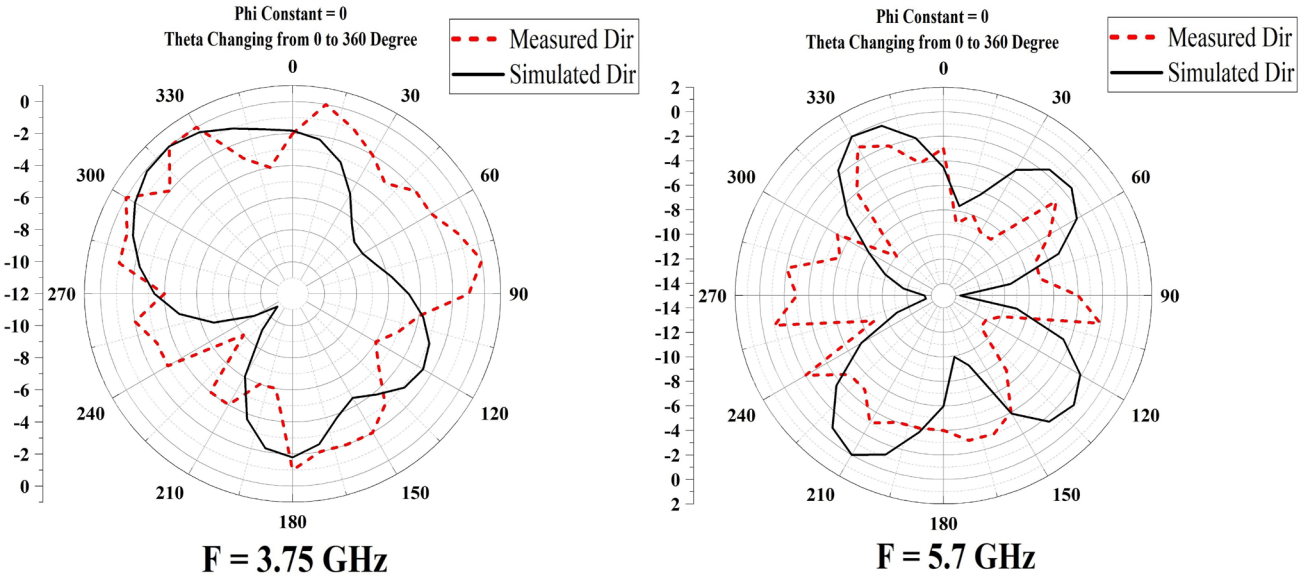

Fig. 16 The normalized 2D radiational pattern for (Antenna-1-d) showed the simulated and the practical measured results

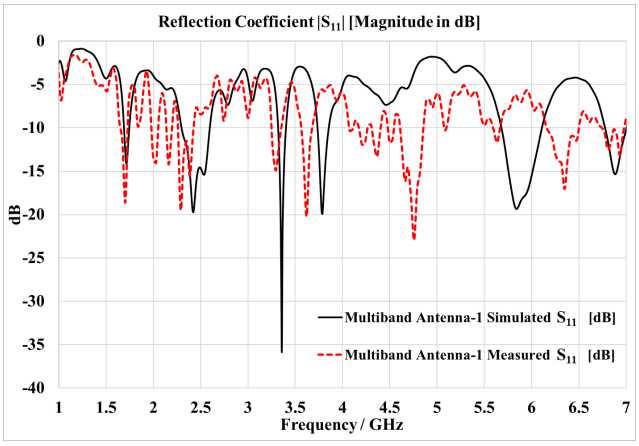

Fig. 17 The Reflection coefficient S_{11} magnitude in [dB] for both the simulated and the practical fabricated (Antenna-1-d)

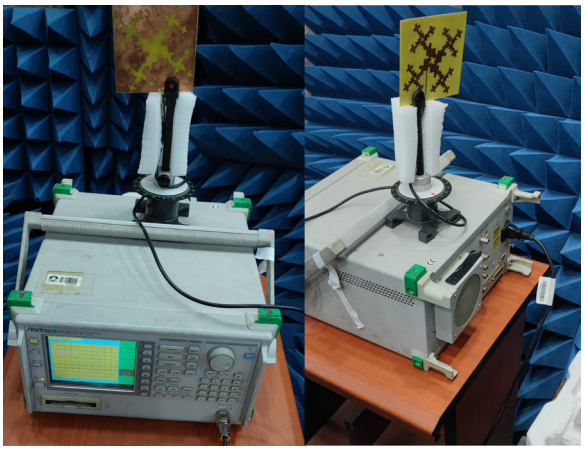

Fig. 18 Testing environment used to measure the normalized 2D radiation pattern for the proposed (Antenna-1-d)

environment since there is no fully anechoic chamber were available in the university where the measurement was recorded. The antenna supports six resonating frequencies (1.7155 GHz, 2.424 GHz, 3.36 GHz, 3.789 GHz, 5.843 GHz, 6.886 GHz) that provides a redundant mechanism for any RF energy harvesting system by supporting variety of wireless services in order to collect more radio frequency ambient energy from different transmitting sources by interface the antenna with the appropriate rectification circuits. Also, the antenna achieves high bandwidth especially for the frequencies 2.4 GHz and 5 GHz, which are the most required frequencies for RF energy harvesting applications.

Table 3 Evaluation of the proposed antenna in this work in comparison to previously published works

Reference	[11]	[13]	[7]	[14]	[4]	This Work
Dimensions	38 mm × 38 mm × 3.2 mm	120 mm × 120 mm × 1.52 mm	60 mm × 60 mm × 60 mm	200 mm × 175 mm × 46.6 mm	120 mm × 120 mm × 30 mm	102.9 mm × 102.9 mm × 1.6 mm
Substrate Type	FR-4	Rogers RT6002	Arlon 25N	Rogers 3003	FR-4	FR-4
Operating Frequency	2.4 GHz	(0.9 – 1.1) GHz, (1.8 – 2.5) GHz	915 MHz, 2.45 GHz	925 MHz, 1.85 GHz, and 2.15 GHz	2.1 GHz, (2.4 – 2.48) GHz, (3.3 – 3.8) GHz	1.7155 GHz, 2.424 GHz, 3.36 GHz, 3.789 GHz, 5.843 GHz, 6.886 GHz
Peak Gain [dBi]	2.2 dBi @ 2.45 GHz	Not available	4.18 dBi @ 2.45 GHz	8.15 dBi @915 MHz, 7.15 dBi @ 1.850 GHz, 8.15 dBi @ 2.15 GHz	7 dBi @ 2 GHz, 5.5 dBi @ 2.5 GHz, 9.2 dBi @ 3.5 GHz	2.785 dBi @ 1.7458 GHz, 2.83 dBi @ 2.45 GHz, –0.79 dBi @ 3.36 GHz, –1 dBi @ 3.856 GHz, 2.51 dBi @ 5.8512 GHz, 2.165 dBi @ 6.886 GHz
Band Width [GHz]	(2.4 – 2.51) GHz	(0.9 – 1.1) GHz, (1.8 – 2.5) GHz	Not available	Not available	(2.4 – 2.48) GHz, (3.3 – 3.8) GHz	(1.6901 – 1.7463) GHz, (2.299 – 2.5978) GHz, (3.3206 – 3.4036) GHz, (3.7373 – 3.8561) GHz, (5.6835 – 6.1116) GHz, (6.7797 – 7.007) GHz,
Remarks	There is just one frequency band supported by the antenna.	The maximum peak gain is not clarified, and it is larger in size.	Only two frequency bands are supported and the thickness is much higher.	larger and thicker, and lacking in supporting WLAN frequency ranges.	It is Bigger in size and significantly thicker.	
The Advantages of our proposed work	Achieved higher gain at 2.45 GHz. and thinner in size and support More frequency bands	More frequency bands are supported, it is smaller in size, and the FR-4 substrate is less expensive than the Rogers RT6002.	FR-4 substrate is less expensive than Arlon 25N, and it is thinner and supports a wider range of frequency bands.	The FR-4 substrate is less expensive than the Rogers 3003, and it is smaller, thinner, and capable of supporting a wider range of frequency bands.	It is thinner and smaller, and it covers a wider range of frequencies.	

References

[1] Ullah, M. A., Keshavarz, R., Abolhasan, M., Lipman J., Esselle, K. P., Shariati, N. "A Review on Antenna Technologies for Ambient RF Energy Harvesting and Wireless Power Transfer: Designs, Challenges and Applications", IEEE Access, 10, pp. 17231–17267, 2022. https://doi.org/10.1109/ACCESS.2022.3149276

[2] Zeng, M., Li, Z., Andrenko, A. S., Zeng, Y., Tan, H. Z. "A Compact Dual-Band Rectenna for GSM900 and GSM1800 Energy Harvesting", International Journal of Antennas and Propagation, 2018(1), 4781465, 2018. https://doi.org/10.1155/2018/4781465

[3] Khemar, A., Kacha, A., Takhedmit, H., Abib, G. "Design and experiments of a dual-band rectenna for ambient RF energy harvesting in urban environments", IET Microwaves, Antennas and Propagation, 12(1), pp. 49–55, 2018. https://doi.org/10.1049/iet-map.2016.1040

[4] Chandravanshi, S., Sarma, S. S., Akhtar, M. J. "Design of Triple Band Differential Rectenna for RF Energy Harvesting", IEEE Transactions on Antennas and Propagation, 66(6), pp. 2716–2726, 2018. https://doi.org/10.1109/TAP.2018.2819699

[5] Yang, L., Zhou, Y. J., Zhang, C., Yang, X. M., Yang, X. X., Tan, C. "Compact Multiband Wireless Energy Harvesting Based Battery-Free Body Area Networks Sensor for Mobile Healthcare", IEEE Journal of Electromagnetics, RF and Microwaves in Medicine and Biology, 2(2), pp. 109–115, 2018. https://doi.org/10.1109/JERM.2018.2817364

[6] Song, C., Huang, Y., Carter, P., Zhou, J., Yuan, S., Xu, Q., Kod, M. "A Novel Six-Band Dual CP Rectenna Using Improved Impedance Matching Technique for Ambient RF Energy Harvesting", IEEE Transactions on Antennas and Propagation, 64(7), pp. 3160–3171, 2016. https://doi.org/10.1109/TAP.2016.2565697

[7] Niotaki, K., Kim, S., Jeong, S., Collado, A., Georgiadis, A., Tentzeris, M. M. "A Compact Dual-Band Rectenna Using Slot-Loaded Dual Band Folded Dipole Antenna", IEEE Antennas and Wireless Propagation Letters, 12, pp. 1634–1637. 2013. https://doi.org/10.1109/LAWP.2013.2294200

[8] Nimo, A., Grgić, D., Reindl, L. M. "Ambient electromagnetic wireless energy harvesting using multiband planar antenna", In: International Multi-Conference on Systems, Signals & Devices, Chemnitz, Germany, 2012, pp. 1–6. ISBN 9781467315906 https://doi.org/10.1109/SSD.2012.6198036

[9] Awais, Q., Jin, Y., Chattha, H. T., Jamil, M., Qiang, H., Khawaja, B. A. "A Compact Rectenna System With High Conversion Efficiency for Wireless Energy Harvesting", IEEE Access, 6, pp. 35857–35866, 2018. https://doi.org/10.1109/ACCESS.2018.2848907

[10] Palazzi, V., Hester, J., Bito, J., Alimenti, F., Kalialakis, C., Collado, A., Mezzanotte, P., Georgiadis, A., Roselli, L., Tentzeris, M. M. "A Novel Ultra-Lightweight Multiband Rectenna on Paper for RF Energy Harvesting in the Next Generation LTE Bands", IEEE Transactions on Microwave Theory and Techniques, 66(1), pp. 366–379, 2018. https://doi.org/10.1109/TMTT.2017.2721399

[11] Shi, Y., Jing, J., Fan Y., Yang, L., Wang, M. "Design of a Novel Compact and Efficient Rectenna for WiFi Energy Harvesting", Progress In Electromagnetics Research C, 83, pp. 57–70, 2018. https://doi.org/10.2528/PIERC18012803

[12] Said, M. A. M., Zakaria, Z., Husain, M. N., Misran M. H., Noor, F. S. M. "2.45 GHz rectenna with high gain for RF energy harvesting", Telkomnika (Telecommunication Computing Electronics and Control), 17(1), pp. 384–391, 2019. https://doi.org/10.12928/TELKOMNIKA.v17i1.11592

[13] Song, C., Huang, Y., Zhou, J., Carter, P., Yuan, S., Xu, Q., Fei, Z. "Matching Network Elimination in Broadband Rectennas for High-Efficiency Wireless Power Transfer and Energy Harvesting", IEEE Transactions on Industrial Electronics, 64(5), pp. 3950–3961, 2017. https://doi.org/10.1109/TIE.2016.2645505

[14] Shen, S., Chiu, C. Y., Murch, R. D. "A Dual-Port Triple-Band L-Probe Microstrip Patch Rectenna for Ambient RF Energy Harvesting", IEEE Antennas and Wireless Propagation Letters, 16, pp. 3071–3074, 2017. https://doi.org/10.1109/LAWP.2017.2761397

[15] Hasan, M. M., Sabaawi, A. M. A. "Microstrip Patch Antenna with Multi-Fins for Radio Frequency Energy Harvesting Applications", Progress In Electromagnetics Research C, 142, pp. 61–73, 2024. https://doi.org/10.2528/PIERC24012803

[16] Hasan, M. M., Sabaawi, A. M. A. "A Modified Fractal Hexagonal Slot Antenna With a Defected Ground Structure for RF Energy Harvesting Applications", International Journal of Microwave and Optical Technology, 19(2), pp. 169–180, 2024.

[17] Mouapi, A. "Radiofrequency Energy Harvesting Systems for Internet of Things Applications: A Comprehensive Overview of Design Issues", Sensors, 22, (21), 8088, 2022. https://doi.org/10.3390/s22218088

[18] Ramya, M., Boopathi Rani, R. "A Compendious Review on Fractal Antenna Geometries in Wireless Communication", In: 2020 International Conference on Inventive Computation Technologies (ICICT), Coimbatore, India, pp. 888–893, 2020. ISBN 9781728146867 https://doi.org/10.1109/ICICT48043.2020.9112580

[19] Sabaawi, A. M. A., Sultan, Q. H., Najm, T. A. "Design and Implementation of Multi-Band Fractal Slot Antennas for Energy Harvesting Applications", Periodica Polytechnica Electrical Engineering and Computer Science, 66(3), pp. 253–264, 2022. https://doi.org/10.3311/PPee.20301

[20] Dassault Systemes "CST Studio Suite 2023.04", [Computer Simulation Technology] Available at: https://www.3ds.com/products/simulia/cst-studio-suite [Accessed: 14 May 2024]

[21] Khandelwal, M. K., Kanaujia, B. K., Kumar, S. "Defected Ground Structure: Fundamentals, Analysis, and Applications in Modern Wireless Trends", International Journal of Antennas and Propagation, 2017, 2018527, 2017. https://doi.org/10.1155/2017/2018527

[22] Balanis, C. A. "Antenna Theory: Analysis and Design", Wiley, 2016. ISBN 978-1-118-642060-1